Numerical and Experimental Investigations on the Flow Field Behind a Complex Distortion Screen

Sivapragasam M.[1*] and Ramamurthy S.[2]

[1]Department of Automotive and Aeronautical Engineering, Faculty of Engineering and Technology
Ramaiah University of Applied Sciences, Bengaluru – 560 058,
[2]Formerly, National Aerospace Laboratories, Bengaluru – 560 017
*Contact Author e-mail: sivapragasam.aae.et@msruas.ac.in

Abstract

The flow field behind a complex distortion screen is investigated numerically and experimentally. The distortion screen was designed using an existing design procedure, and was fabricated by water-jet cut technique. The distorted total pressure field behind the screen was quantified by a Distortion Index parameter, which was evaluated from computations and experiments for several values of inlet Mach number. The root-mean-square error between the target total pressure values at the Aerodynamic Interface Plane and that achieved by the screen design was 4.75 %. A detailed interpretation of the distorted total pressure field is made by means of defining a total pressure flux existing behind the screen. It is seen that the circumferential vorticity is a major contributing factor to the total pressure flux.

Key Words: Total Pressure Distortion, Distortion Screen, Distortion Index, Total Pressure Flux

1. INTRODUCTION

The performance of a gas turbine engine is adversely affected by the non-uniform or distorted flow in the aircraft inlet duct. The compressors are designed for uniform flows and suffer from performance degradation due to distorted inflow conditions leading the compressor to aerodynamic instabilities like rotating stall and surge. Inlet flow distortion also lowers the surge margin of the compressor. The distortion in the inlet flow field can be of static or total pressure, or temperature, or velocity. The total pressure distortion is the most common type and also has the most deleterious effect on the performance of the compressor. The total pressure distortion can be either in circumferential or radial directions and such total pressure patterns are called 'classical' distortion patterns. The total pressure distortion profiles such as those occurring in flight conditions are termed 'complex' distortion patterns and can have both circumferential and radial non-uniformities. Distortion screens are commonly employed for simulating total pressure distorted inlet flow field in ground test facilities. The screens are simply wire meshes of various porosities secured to a frame and placed ahead of the engine/compressor. The screen porosities are chosen to produce the required pressure drop. The general subject of inlet flow field distortion and its adverse effects on the performance and stability of compression systems were reviewed in Sivapragasam and Ramamurthy [1].

In the present paper the flow field behind a complex distortion screen is investigated experimentally and computationally. The results are presented in terms of the total pressure field and comparison is made with the target data. Further, a detailed interpretation of the distorted total pressure field is made by means of defining a total pressure flux existing behind the screen.

2. DISTORTION SCREEN

The design of the distortion screen is covered in Sankaranarayanan et al. [2]. Briefly, a series of systematic experiments were conducted to characterise the screen meshes of various porosities in terms of their loss coefficients and distortion parameters, and a comprehensive database was generated. Based on the experimental studies and the database accumulated, an inverse design methodology was developed to design a mesh combination for producing a prescribed total pressure distortion pattern.

During the course of this work, it was found that the distortion screen assembly made from wire mesh presented a number of fabrication and operational difficulties. The screen assembly was fabricated from a combination of wire meshes cut to the required shape and stitched and welded at the intersecting planes. This fabrication technique required high skill and was executed with great care. The welded regions created large blockage to the flow path and caused excessive pressure drop across them. Due to different gauze wires welded near the joints, the mechanical strength of the joints was weak. This required installation of additional thick mechanical guards to prevent the ingestion of wire mesh into the engine on test should they fail. Moreover, the wire meshes of required porosity calculated by the inverse method were not available commercially. This forced the use of commercial mesh close to the design specification and settle for a compromise on the obtained total pressure pattern.

These difficulties were overcome by a new manufacturing technique evolved by Ramamurthy et al. [3]. In this technique, different porosity holes were cut on a single stainless steel sheet by a laser beam. By suitably selecting the holes size and web width, any required porosity could be achieved. The screens were

carefully designed to withstand the required mechanical strength by properly designing the web width. This avoided the need for guards downstream of the screen. Since this screen had no joints, the excessive flow blockage was eliminated. During manufacturing of several laser-cut screens, it was found that the thin stainless steel sheet had warped due to the tremendous heat generated by the cutting action of the laser beam. This problem was overcome by choosing to cut the square holes of required size by a water-jet. This technique was highly successful in fabricating warp-free distortion screens. One such screen designed and fabricated by this method is chosen for the present study and is shown in Fig. 1.

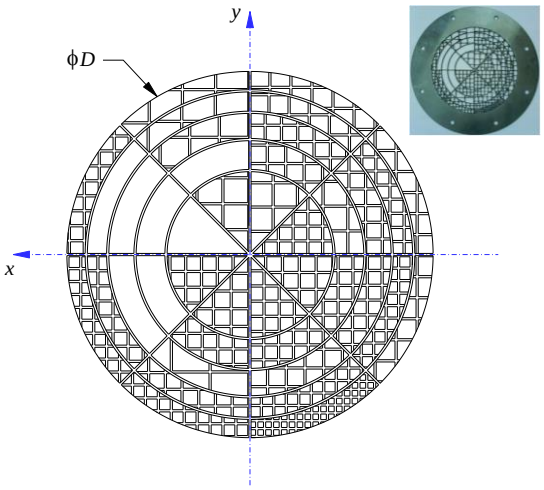

Fig. 1 Distortion screen used in the present study. Inset: Photograph of screen fabricated by water-jet cut technique.

3. COMPUTATIONAL PROCEDURE

The computational domain was a circular cylinder whose diameter was D = 102 mm. The length of this computational domain extended 2 D upstream of the screen and 5 D downstream of the screen. The thickness of the screen was 2 mm. The distorted flow field was evaluated at z/D = 0.294 downstream of the screen. This plane is reckoned to be the Aerodynamic Interface Plane (*AIP*) which is used to define the total pressure distortion between the aircraft inlet and engine. The computational domain had a total of 2,087,478 grid points. At the inlet of the computational domain total and static pressure boundary conditions were imposed and at the outlet the static pressure was specified. The total temperature was specified at the inlet and the outlet of the computational domain. The no-slip boundary condition was applied on the screen and on the wall of the cylindrical computational domain. The Reynolds-averaged Navier-Stokes equations are solved numerically using the commercial finite-volume method based code ANSYS FLUENT. Spatial discretization was done by a formally second-order accurate numerical scheme, and pressure-velocity coupling was achieved by the SIMPLE algorithm. Turbulence closure was achieved by using the standard k-ε turbulence model. All calculations were carried out in double-precision arithmetic. The computations were performed for a range of inlet Mach numbers, M_1, from 0.06 to 0.48.

4. EXPERIMENTAL PROCEDURE

An experimental facility was designed and built to study the characteristics of distortion screens and is shown in the Fig. A1 in the Appendix. The primary air stream is supplied by a centrifugal blower, passing through a diffuser, settling chamber which consists of honeycomb and turbulence reduction screens, contraction and then entering the test section. The air mass flow rate can be controlled by a conical throttle at the exit of the straight duct which can be moved axially by means of a lead screw and a nut. M_1 was calculated by measuring the total and wall static pressures and total temperature at a location 3.12 D upstream of the screen. The total pressure field behind the screen was measured at five axial locations behind the screen using forty total pressure probes. These probes were arranged in eight equi-angularly spaced rakes, each rake consisting of five probes located at the centres of equal annular ring areas of the duct in accordance with AIR 1419 [4]. The pressures were measured by ESP-32HD miniature electronic differential pressure scanners. The signals from the transducers were acquired by an Agilent 34970A Data Acquisition/Switch Unit through RS-232 interface and a data acquisition program was used to acquire and process the experimental data. The turbulence intensity at the inlet of the test section was measured by a hot-wire anemometer (DANTEC 55P11 system) and was found to be 0.3 %. This value was imposed as turbulence boundary condition for the computations.

5. RESULTS AND DISCUSSION

The total pressure non-uniformity can be quantified by means of a parameter Distortion Index *DI*, which is defined as,

$$DI = \frac{p_{0,\max} - p_{0,\min}}{p_{0,ave}} \qquad (1)$$

where $p_{0,\max}$ and $p_{0,\min}$ are the maximum and minimum total pressures, respectively, and $p_{0,ave}$ is the average total pressure in any plane of interest. The distortion indices were calculated from the total pressures at five axial locations behind the screen, and a typical result at the *AIP* (z/D = 0.294) is shown in Fig. 2. The computational results agree well with the experimental data at all the planes. The *DI* values increase with an increase in M_1. The maximum values of *DI* were observed at the plane just downstream of the screen at z/D = 0.294 till M_1 = 0.458. At higher values of M_1, maximum values of *DI* occurred at an aft plane (z/D = 0.706). At M_1 = 0.458 most of the holes in the screen are choked except for the larger ones. With further increase in M_1 a steep rise in *DI* is observed.

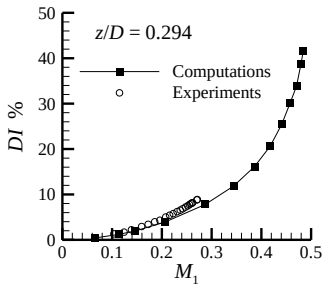

Fig. 2 Distortion Index at *AIP* (*z*/*D* = 0.294).

The screen design is able to reproduce the target distortion pattern well. The difference in the total pressure pattern can be quantified in terms of a root-mean-square error (*RMSE*) defined as,

$$RMSE = \sqrt{\frac{\sum_{i=1}^{n}\left(\frac{p_{0,\,obtained}}{p_{0,\,target}} - 1\right)^2}{n}} \times 100\ \% \tag{2}$$

where n = 40 is the number of sampling points. The *RMSE* between the target total pressure values at the *AIP* and that achieved by the screen design was 4.75 %.

An alternate and a detailed interpretation of the distorted total pressure field can be made in terms of total pressure flux defined as follows (see, Guo et al. [5] and Yang et al. [6]),

$$\mathrm{P} = \int_S p_0\, u_z\, dS \tag{3}$$

where S is the cross-sectional plane. This quantity would be the total pressure flux that would be existing behind the screen and that would subsequently enter the downstream compressor. The term on the LHS of eq. (3) can be rewritten in the framework of derivative-moment transformation (DMT) advanced in Wu et al. [7,8]. The key idea behind the DMT is the extension of integration by parts to two- and three-dimensions using the Gauss and Stokes theorems. For example, for any scalar φ, the integral of any normal vector $\varphi\boldsymbol{n}$ over an open surface S bounded by a closed loop C can be written as,

$$\int_S \varphi\boldsymbol{n}\, dS = -\frac{1}{k}\int_S \boldsymbol{x}\times(\boldsymbol{n}\times\nabla\phi)dS + \frac{1}{k}\oint_C \phi\,\boldsymbol{x}\times d\boldsymbol{x} \tag{4}$$

where k denotes the spatial dimensionality. If S is a closed surface, the second term on the RHS of eq. (4) vanishes. Using eq. (4), we can write

$$\int_S p_0\, u_z\, \boldsymbol{e}_z\, dS = -\frac{1}{2}\int_S \boldsymbol{r}\times(\boldsymbol{e}_z\times\nabla\, p_0\, u_z)dS \quad . \tag{5}$$

At this stage, we write the radial component of the steady momentum equation in vortical form as below:

$$\frac{\partial p_0}{\partial r} = -\rho(\omega_\theta u_z - \omega_z u_\theta) - \mu\left(\frac{1}{r}\frac{\partial \omega_z}{\partial \theta} - \frac{\partial \omega_\theta}{\partial z}\right) \tag{6}$$

where ρ is the density, μ is the coefficient of viscosity, u is the velocity, ω is the vorticity, and r, θ and z represent the radial, circumferential and axial components, respectively, in the cylindrical coordinate system. Expanding eq. (5), and using eq. (6), we obtain,

$$\int_S p_0\, u_z\, dS = \frac{1}{2}\int_S r\,\rho\,\omega_\theta\, u_z^2\, dS + \frac{1}{2}\int_S r\, p_o\, \omega_\theta\, dS$$
$$-\frac{1}{2}\int_S r\,\rho\, u_z\, u_\theta\, \omega_z\, dS - \frac{1}{2}\int_S r\, p_0\frac{\partial u_r}{\partial z}\, dS + \frac{1}{2}\int_S r\, u_z\, \psi\, dS \tag{7}$$

where ψ is the viscous term. The integrals on the RHS of eq. (7) have detailed information concerning the contributions to the total pressure flux. We evaluated these integrals from the computations for $M_{ave,\ AIP}$ = 0.577, and present in Fig. 3. In Fig. 3, the five integrals on the RHS of eq. (7) are denoted as I_i, where i = 1 to 5.

First, we discuss the behaviour of the total pressure flux, P, as defined in eq. (3). The average total pressure at any plane perpendicular to the axis of the duct represented by $\int p_0\, dS$ continuously decreases due to friction from the inlet till the plane of the screen, and there is a rapid drop across the screen, and further decrease in the duct downstream of the screen. However, the $\int u_z\, dS$ term increases in the region ahead of the screen, again due to friction, a steep increase across the screen, and further increase downstream of the screen. Thus, $\int p_0\, u_z\, dS$, behaves the way we see in Fig. 3. The major contributors to P are the I_1, I_2, and I_4 terms signifying the importance of the circumferential vorticity ω_θ and the axial gradient of radial velocity component $\partial u_r/\partial z$. Further, since $|u_z| >> |u_r|$, $|u_\theta|$, and also $|\omega_\theta| >> |\omega_r|$, $|\omega_z|$, the I_3 term becomes small. The viscous term, I_5, is negligible.

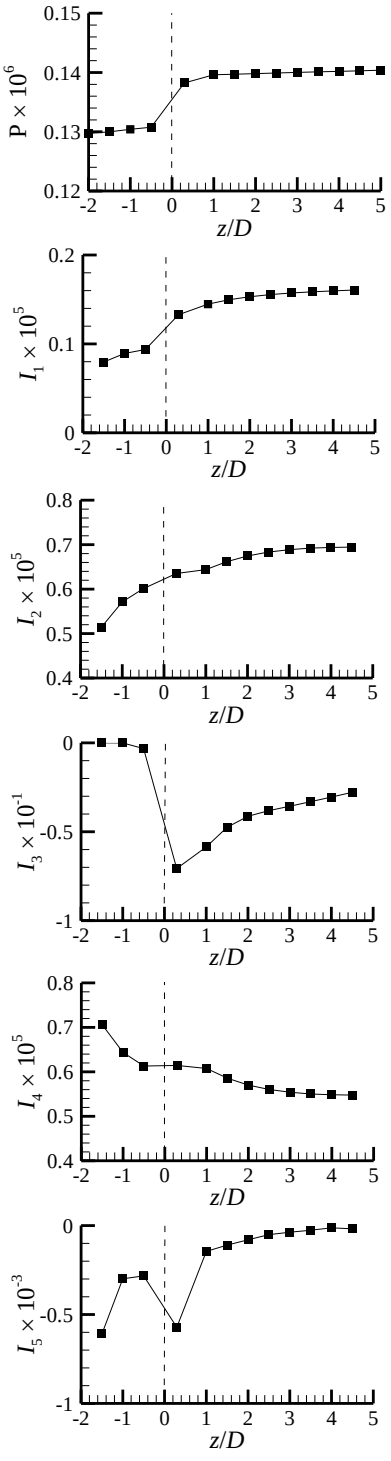

Fig. 3 Integrals in eq. (7); note the different scales on the *y*-axes. The screen is at *z*/*D* = 0, denoted by a vertical dashed line, and the *AIP* is at *z*/*D* = 0.294.

6. CONCLUSION

The total pressure field behind a complex distortion screen was studied numerically and experimentally. The total pressure distortion was quantified by a Distortion Index parameter. Highest values of this parameter occurred at the Aerodynamic Interface Plane till the inlet Mach number = 0.458. The root-mean-square error between the target total pressure values at the *AIP* and that achieved by the screen design was 4.75 %. A detailed interpretation of the total pressure field was also made in terms of a total pressure flux parameter. This parameter was further expanded using the derivative moment transformation technique. The terms thus arising contain detailed information about the individual contributions to the total pressure flux. The integral terms containing the circumferential vorticity ω_θ and the axial gradient of radial velocity component $\partial u_r/\partial z$ are the major terms contributing to the total pressure flux quantity. This information will be useful for screen designers and compressor aerodynamicists.

REFERENCES

[1] Sivapragasam, M., Ramamurthy, S., (2009) Inlet Flow Distortion Effects in Aircraft Gas Turbine Engine Compression Systems, NAL TM PR0901, Bangalore: National Aerospace Laboratories.

[2] Sankaranarayanan S., Murugesan K., Rao K.V.L., (1994) Simulation of Distorted Flow Through an Engine Intake Using Mesh Combinations, *Air Breathing Engines and Aerospace Propulsion*, Bangalore: Interline Publishing.

[3] Ramamurthy S., Murugesan K., Sankaranarayanan S., Ramachar D., (1998) Design and Development of Distortion Screens for a Gas Turbine Engine Intake, *Air Breathing Engines and Aerospace Propulsion*, Bangalore: Interline Publishing.

[4] Society of Automotive Engineers, (1999) Inlet Total-Pressure-Distortion Considerations for Gas-Turbine Engines, SAE AIR 1419.

[5] Guo M., Li Q., Hou A., Yuan W., (2006) A Diagnostic and Design Approach of Axial Compressor Based on Local Dynamics, ASME GT2006-91116.

[6] Yang Y., Wu H., Li Q., Zhou S., Wu J.Z., (2008) Vorticity Dynamics in Axial Compressor Flow Diagnosis and Design, ASME J. Fluids Eng., 130, 041102.

[7] Wu J.Z., Ma H.Y., Zhou M.D., (2006) *Vorticity and Vortex Dynamics*, Berlin: Springer-Verlag.

[8] Wu J.Z., Ma H.Y., Zhou M.D., (2015) *Vortical Flows*, Berlin: Springer-Verlag.

APPENDIX

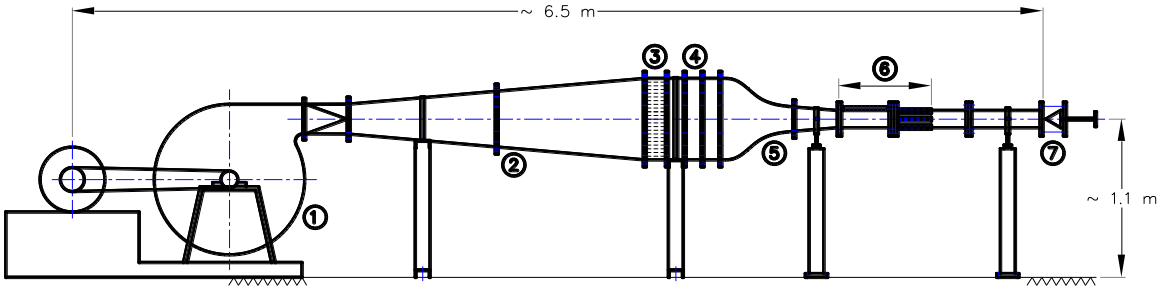

Fig. A1 Layout of the test facility; the major components are numbered and are (1) centrifugal blower, (2) diffuser, (3) honeycomb, (4) screens, (5) contraction, (6) test section and (7) exit throttle.